Article:
Fong, W-K, Sanchez-Ferrer, A, Rappolt, M et al. (2019) Structural transformation in vesicles upon hydrolysis of phosphatidylethanolamine and phosphatidylcholine with phospholipase C. Langmuir, 35 (46). acs.langmuir.9b02288. pp. 14949-14958. ISSN: 0743-7463

https://doi.org/10.1021/acs.langmuir.9b02288

Structural transformation in vesicles upon hydrolysis of phosphatidylethanolamine and phosphatidylcholine with phospholipase C

Wye-Khay Fong[a,b,c*1], Antoni Sánchez-Ferrer[a], Michael Rappolt[d], Ben J. Boyd[b] and Raffaele Mezzenga[a*]

[a]ETH Zürich, Department of Health Sciences & Technology, 8092 Zürich, Switzerland; [b]Drug Delivery, Disposition and Dynamics, and ARC Centre of Excellence in Convergent Bio-Nano Science and Technology, Monash Institute of Pharmaceutical Sciences, Monash University, Parkville Campus, 381 Royal Parade, Parkville, VIC 3052, Australia. [c]Adolphe Merkle Institute, University of Fribourg, Chemin des Verdiers 4, 1700 Fribourg, Switzerland. [d]School of Food Science and Nutrition, University of Leeds, LS2 9JT, United Kingdom

[*]Raffaele.mezzenga@hest.ethz.ch & khay.fong@newcastle.edu.au

Abstract

This study provides insight into dynamic nanostructural changes in phospholipid systems during hydrolysis with phospholipase C, the fate of the hydrolysis products and the kinetics of lipolysis. The effect of lipid restructuring of the vesicle was investigated using small-angle X-ray scattering and cryogenic scanning electron microscopy. The rate and extent of phospholipid hydrolysis was quantified using NMR. Hydrolysis of two phospholipids, phosphatidylethanolamine and phosphatidylcholine, results in the cleavage of the molecular headgroup, causing two strikingly different changes in lipid self-assembly. The diacylglycerol product of phosphatidylcholine escapes the lipid bilayer, whereas the diacylglycerol product adopts a different configuration within the lipid bilayer of the phosphatidylethanolamine vesicles. These results are then discussed concerning the change of lipid configuration upon the lipid membrane and its potential implications *in vivo*, which is of significant importance for the detailed understanding of the fate of lipidic particles and the rational design of enzyme-responsive lipid-based drug delivery systems.

Abbreviations

PLC – phospholipase C; sPC – soy phosphatidylcholine; ePE – egg phosphatidylethanolamine;

DAG – diacylglycerol; L_α – lamellar phase; H_{II} – inverse hexagonal phase.

Introduction

In the search for better medical treatments, lipid-based drug delivery systems have been used to improve therapeutic outcomes. However, the *in vivo* fate of these materials is still unclear. Lipid hydrolysis is an important process for the absorption of nutrients and cellular signalling. There remains considerable uncertainty about basic enzyme function and consequently, the mechanism of lipolysis as well as the malfunction of lipases in disease states such as obesity, diabetes, and atherosclerosis. Additionally, the solubility of some lipid soluble drugs and nutrients are intrinsically linked to the fate of the drug delivery formulation and drug distribution is dictated by the type of colloidal phases generated during digestion.[1-3]

Nanostructured lipid particles can be designed, built and applied as vehicles for stimuli responsive drug delivery. By switching between the different self-assembled mesophases, the inherent release rates of each nanostructure can be utilised.[4-7] Additionally, the formation of complex inverse nanostructures is implicated in the promotion of membrane fusion. Thus, understanding the way that lipidic particles are processed in the body is key to their therapeutic application. The action of lipases upon lipid self-assembly during intestinal digestion are important in directing the absorption of fat-soluble drugs and nutrients. Lipolysis has been shown to modify the self-assembly of a range of different commonly encountered lipid colloids, where the extent and direction of the reaction is also contingent on the presence of bile salts and pH.[8] For instance, emulsions formed by medium chain triglycerides transition to vesicles upon digestion;[9] monoolein based cubosomes transition from inverse cubic through a variety of inverse nanostructures to dispersed oil droplets upon hydrolysis;[10] milk emulsions (triglycerides) transition to a variety of differently ordered nanostructures.[8, 11] The selective lipolysis of lipids from the interface of lipidic particles can also direct the phase transitions,[12-13] where the products of hydrolysis align themselves within the lipid bilayer according to their physicochemical properties.[14]

Towards the development of enzyme-responsive lipid-based nanomaterials as drug delivery systems, this study seeks to understand the changes in nanostructure of phosphatidylcholine (PC) and phosphatidylethanolamine (PE) based particles under the action of phospholipase C (PLC); an interfacially active enzyme that was until recently viewed only as an instrument of lipidic degradation. The role of PLC in physiology is well understood,[15-16] however, it is the discovery of role of PLC in disease states[17-18] that has renewed interest in the *in vivo* function of phospholipase C and painted them as a target for drug delivery.

Both PE and PC are extensively used in different ratios in the formulation of liposomal drug delivery products, however the molecular mechanisms of their respective roles in the final delivery to the site of action is not completely understood. The site of PE and PC cleavage by three types of phospholipases are shown schematically in Fig. 1. Thus, in this study, lipolysis as a mediator for triggered drug release and vesicle fusion was investigated. As the different phospholipids play different

roles both in lipid homeostasis, as well as drug delivery, it is important to study the dynamic behaviour of these formulations in order to understand both the contradictory events of unexpected drug release and the enhancement of drug release by this mechanism.

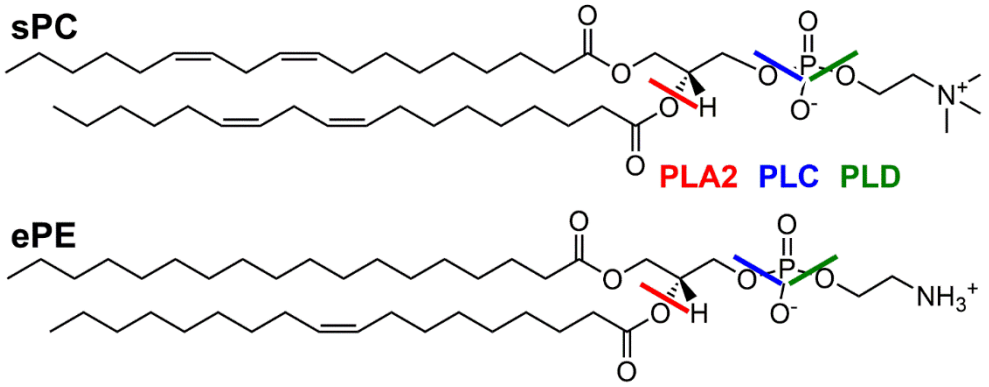

Fig. 1 – Representative molecular structures of the major components of soy phosphatidylcholine (sPC) and egg phosphatidylethanolamine (ePE) utilised in this study. The coloured bars represent the location of molecular cleavage catalysed by different phospholipases (PL): PLA2 (red), PLC (blue) and PLD (green). This study focuses on the action of phospholipase C (PLC).

Experimental

Materials

Egg phosphatidylethanolamine (ePE) and soy phosphatidylcholine (sPC) Lipoid S100 were obtained from Lipoid AG (Switzerland); compositions are detailed in Table 1. Phospholipase C from *Bacillus cereus*, dipotassium hydrogen phosphate and calcium chloride were purchased from Sigma Aldrich. Dilinolein (dilinoleoylglycerol) was purchased from Nu-Chek Prep (MN, USA). Sodium chloride and sodium dihydrogen phosphate were purchased from Merck. Pluronic F127, a hydrophilic tri-block copolymer (PEG-PPG-PEG), was obtained from BASF SE (Germany).

Table 1 – Fatty acid composition of the phospholipid tails used in this study, as provided by Lipoid AG. Average number of unsaturations were determined via 1D ^{1}H and ^{13}C NMR.

Fatty acid		**ePE (%)**	**sPC (%)**
Palmitic	C16	30-35	12-17
Stearic	C18	10-15	2-5
Oleic	C18:1	30-38	7-12
Linoleic	C18:2	12-18	59-70
Linolenic	C18:3	-	5-8
Unsaturations/molecule[a]		1	4

[a] Average number of unsaturations per phospholipid molecule evaluated from the chemical composition and confirmed by ^{1}H NMR.

Lipid dispersions

Phospholipids were weighed into round bottom flasks and dissolved in a dichloromethane:methanol (2:1) mixture. Thin films of phospholipids were then formed by removing the solvent via rotary evaporation. For the dynamic studies, the lipid films were formed with either ePE or sPC only (5% w/v). For the equilibrium studies, the lipid films were formed by incorporating a model diacylglycerol, dilinolein, which is the major component from sPC hydrolysis, in defined molar ratios. The lipids were then hydrated in phosphate buffered saline (PBS) (5 wt% lipid, 50 mM phosphate buffer, pH 7.4) or in PBS containing Pluronic F127 (0.5 wt% F127, 5 wt% lipid, 50 mM phosphate buffer, pH 7.4) to form vesicles. The coarse dispersions were further processed by ultrasonication (10 min pulsed, 30% amplitude) in order to reduce and homogenise the particle size.

Small angle X-ray scattering (SAXS)

SAXS was used to investigate the aggregates formed in equilibrium mixtures. Experiments were performed using a Rigaku S-Max 3000 SAXS system (Japan) equipped with a copper-target micro focus X-ray tube MicroMax-002$^+$ (45 kV, 0.88 mA). The Ni-filtered Cu Kα radiation ($\lambda_{\text{Cu K}\alpha}$ = 1.5418 Å) was collimated by a three pinhole collimator (0.4, 0.3 and 0.8 mm in diameter), and the data were collected by a two dimensional argon-filled Triton-200 X-ray detector (Rigaku, Japan; 20 cm diameter, 200 µm resolution). An effective scattering-vector range of 0.006 Å^{-1} < q < 0.4 Å^{-1} was investigated, where q is the scattering wave-vector defined as $q = 4\pi \sin\theta/\lambda_{\text{Cu K}\alpha}$, with a scattering angle of 2θ. For all measurements, the samples were filled into a 1.5 mm internal diameter quartz capillary and sealed with epoxy glue. Measurements were performed at 37 °C, where samples were equilibrated for 30 min prior to measurements. The scattered intensity was collected over 2.5 h.

Time-resolved synchrotron SAXS: *In vitro* digestion experiments were conducted using a thermostated glass digestion vessel at 37 °C, fitted with tubing to enable flowthrough scattering analysis to be conducted in real time.[19] To 7 mL of lipid dispersion in the glass vessel, 0.5 mL of a 1 mg·mL^{-1} phospholipase C solution in PBS was added using a remotely driven syringe pump, while the digesting medium was pumped through a 1.5 mm quartz capillary flow cell at 10 mL·min^{-1} using a peristaltic pump. The quartz capillary was placed in the X-ray beam at the SAXS/WAXS beamline at the Australian Synchrotron.[20] Scattering profiles were acquired for 5 s every 10 s at an energy of 10 keV using a Pilatus 1 M detector (Dectris, Switzerland; active area 169 × 179 mm^2 with a pixel size of 172 µm) with a sample-to-detector distance of 1.6 m providing a q-range of 0.01 < q < 0.6 Å^{-1}, where q is the length of the scattering vector defined by $q = 4\pi \sin\theta/\lambda$, with λ being the wavelength and 2θ the scattering angle. The scattering images were integrated into the one-dimensional scattering function $I(q)$ using the in-house developed software package ScatterBrain. The q-range calibration was made using silver behenate as the standard. The liquid crystalline space groups and lattice parameters (a)

were determined by the relative positions of the Bragg peaks in the scattering curves, which correspond to the reflections on planes defined by their (*hkl*) Miller indices.[21]

As the quality of the diffraction data of these multi-component and multi-colloidal systems was limited by experimental constraints, both simple bilayer models (sPC samples), as well as classical Fourier synthesis (ePE samples), were utilised to estimate the bilayer thickness in the fluid lamellar phases.[22-23] Briefly, after background subtraction, all diffraction peaks were fitted with Lorentzian distribution using Origin 2016, and finally, the resulting intensities, I_h, were Lorentz corrected in order to obtain the form factor values F_h (for details see reference 22 and therein). The electron bilayer profiles (EDP) were then determined by (Fig. SI-1):

$$\Delta\rho(z) = \sum_{h=1}^{h\ max} \alpha_h \,.F_h \,.\cos(\frac{2\pi hz}{d}) \quad (1)$$

Where h is the Miller index, α_h are the phases, F_h are the form factors, and d denotes the d-spacing of the lattice and z is the distance in real space. sPC bilayers were estimated by the 'two-peak method' detailed in reference,[23] which utilises the experimental form factors, F_1 and F_2, and average material parameter values from literature to estimate the head group at the positions $\pm z_H$. For comparison, a modified Luzzati method [24] for determining bilayer dimensions was also considered, but the latter results are only discussed in the Supplementary Information together with the results of the 'two-peak method'.

The structural parameters of the H_{II} phase formed by ePE and ePE/F127 were estimated from electron density maps calculated by standard Fourier synthesis according to reference [25]. Since only the first three orders were recorded throughout, *i.e.*, the (10), (11) and (20) reflections, the deduced mean head-group position, R_H (for definition, see Figure SI-2) is underestimated. Note, from such low resolution electron density maps the true electron density position R_H* can only be estimated following the method of reference [25]. The following equations were applied:

$$R_H^* = 1.12\ R_H \quad (2)$$

$$a = 2\ R_H^* + d_{HH} \quad (3)$$

$$2\ R_W = 2\ R_H^* - 11\ \text{Å} \quad (4)$$

Where a is the lattice parameter, R_H is experimental head group radius, d_{HH} is the shortest head to head group distances (for definitions see Figure SI-2), R_W is the water core radius and 11 Å is a commonly applied estimation of the radial head group extension.[25]

Nuclear Magnetic Resonance (NMR)

To evaluate the composition of the products of phospholipid hydrolysis, 1D ^{1}H and ^{13}C NMR experiments, as well as DEPT and 2D ^{1}H-^{1}H (COSY) and ^{1}H-^{13}C (HETCOR) NMR experiments were

carried out on a Bruker Advance spectrometer (Bruker BioSpin GmbH, Rheinstetten, Germany), operating at 400 MHz (^{1}H) and 100 MHz (^{13}C), and using D_2O or DMSO-d_6 as solvents and as internal standards. Example NMR spectra are presented in the ESI (Fig. SI-2).

The process of hydrolysis was quantified by ^{1}H NMR by following the apparition and evolution of a peak (quintuplet) at δ = 5.08 ppm, which corresponds to a single H in C2 from the glycerine moiety, upon hydrolysis of the phosphate ester between the phosphatidic acid and glycerol moiety. The integrated area was normalized taking into account the constant area corresponding to the peak (multiplet) at δ = 0.87 ppm of the two terminal CH_3 groups in the fatty tails. Data were fitted to consider an increase in particle size over time (Table SI-2) as per equation (5), where *H* refers to the extent of reaction, *t*, time in minutes and k_i the rate of hydrolysis.

$$H(t) = H_{max} \sum_{i=1}^{2} H_i \left(1 - e^{-k_i t}\right) \quad (5)$$

Cryogenic scanning electron microscopy (cryoSEM)

Approx. 6 µL of the lipid dispersions (5% w/v, 7 mL) undergoing PLC catalysed hydrolysis (0.5 mL of a 1 mg·mL^{-1}) were loaded into aluminium half shells and then frozen under high pressure (2100 bar) with liquid nitrogen and within milliseconds using the Bal-Tec HPM100 (Leica) high-pressure freezing system. Rapid freezing prevents the formation of ice crystals which otherwise would have affected the delicate nanostructure of the liquid-crystalline nanoparticles. Flash freezing the samples in real time also arrests the action of the enzymes whilst avoiding the use of enzyme inhibitors, which may alter the ultrastructure of the particles. Using a freeze-fracture system (BAF 060, Baltec) the samples were fractured with a diamond knife and coated with 6 nm of tungsten in the frozen state in order to prevent surface charging during imaging. A cryo-transfer device was then used to transport the frozen material to a SEM instrument (Zeiss Leo 1530).

Results

The hydrolysis of the vesicles formed by the two phospholipids resulted in vastly different dynamic phase behaviour driven by the reduction in headgroup size to form diglycerides. Specifically, the diacylglyceride products (DAG1 and DAG4 from ePE and sPC, respectively; numbers refer to the average number of unsaturations in the lipidic tail as shown in Table 1) can influence the self-assembly of the lipids at the interface due to their specific amphiphilic nature. The dynamic transformation of structure was followed by synchrotron SAXS and cryoSEM, and changes in composition was followed by NMR. These results were then compared to equilibrium structural studies as determined by SAXS.

Structural changes resulting from PLC catalysed hydrolysis egg phosphatidyl-ethanolamine (ePE)

The structural evolution caused by hydrolysis of dispersed ePE, both with a polymeric stabiliser (Pluronic F127) (ePE/F127) and without (ePE), were followed by time-resolved synchrotron SAXS (Fig. 2 and Fig. SI7). The phase transitions of ePE and ePE/F127 were very similar: $L_\alpha \rightarrow L_\alpha + H_{II} \rightarrow H_{II} \rightarrow$ fluid isotropic $\rightarrow$ unstructured emulsion and/or aggregation. However, they differ in the timing of the phase transitions and colloidal stability. It is noted that in the absence of the enzyme, there was no change in the ePE dispersion over time, *i.e.*, the fluid lamellar phase L_α was conserved over the entire observation period of half an hour (Fig. SI-4A). The phase transitions and timing of the PLC catalysed hydrolysis are as follows:

ePE: $L_\alpha \rightarrow L_\alpha + H_{II}$ (175 s) $\rightarrow H_{II}$ (350 s) $\rightarrow 2 \times H_{II}$ (405 s) $\rightarrow$ unstructured emulsion (636 s). Even with constant agitation, the flow of the sample became blocked due to aggregation of the lipid particles after 700 s. This is attributed to the loss of the charged moieties on the PE headgroup that initially provide electrostatic stability of the dispersion, but its loss then contributes to the dominating fusogenic nature of DAGs.[26] The second H_{II} phase is minor compared to the main H_{II} phase; the dual phases are highlighted in Fig. SI7. The presence of multiple H_{II} phases may be an indication of particle aggregation preventing full access of the enzyme to its substrate.

ePE/F127: $L_\alpha \rightarrow L_\alpha$ + micelles (147 s) $\rightarrow L_\alpha + H_{II}$ (386 s) $\rightarrow H_{II}$ (828 s) $\rightarrow$ fluid isotropic (1610 s) $\rightarrow$ unstructured emulsion (1653 s). As the dispersion containing the non-ionic surfactant was more colloidally stable during hydrolysis, it was further investigated using cryoSEM (Fig. 3). The timing and evolution of images are: (1) 30 s unilamellar vesicles, (2) 315 s multilamellar onion-like vesicles, (3) 611 s striations consistent with the inverse micellar rods of H_{II}, as well as multilamellar vesicles, (4) 1800 s fluid isotropic phase, and (5) 3610 s unstructured emulsion.

Changes in the structural changes in bilayer and water spacings are shown in Fig. 2, right (for derivations see SI pages 1-3). Both the ePE and ePE/F127 formulations demonstrated almost identical changes over time, albeit at different times. As the ePE dispersion was hydrolysed, a slight increase in L_α bilayer thickness, d_{HH}, and reduction of L_α water layer thickness, d_W, was observed, attributed to both the incorporation of a finite amount of DAG1 into the hydrophobic tail region and the reduction of bound water to the hydrolysed headgroups. The transition to the H_{II} phase was accompanied by the reduction of d_{HH} by ~3.7 Å and an increase in free water, as has been observed with an increase in temperature.[25] Note, the significant decrease in d_{HH} is expected due to the increase of chain splay in the H_{II} phase.

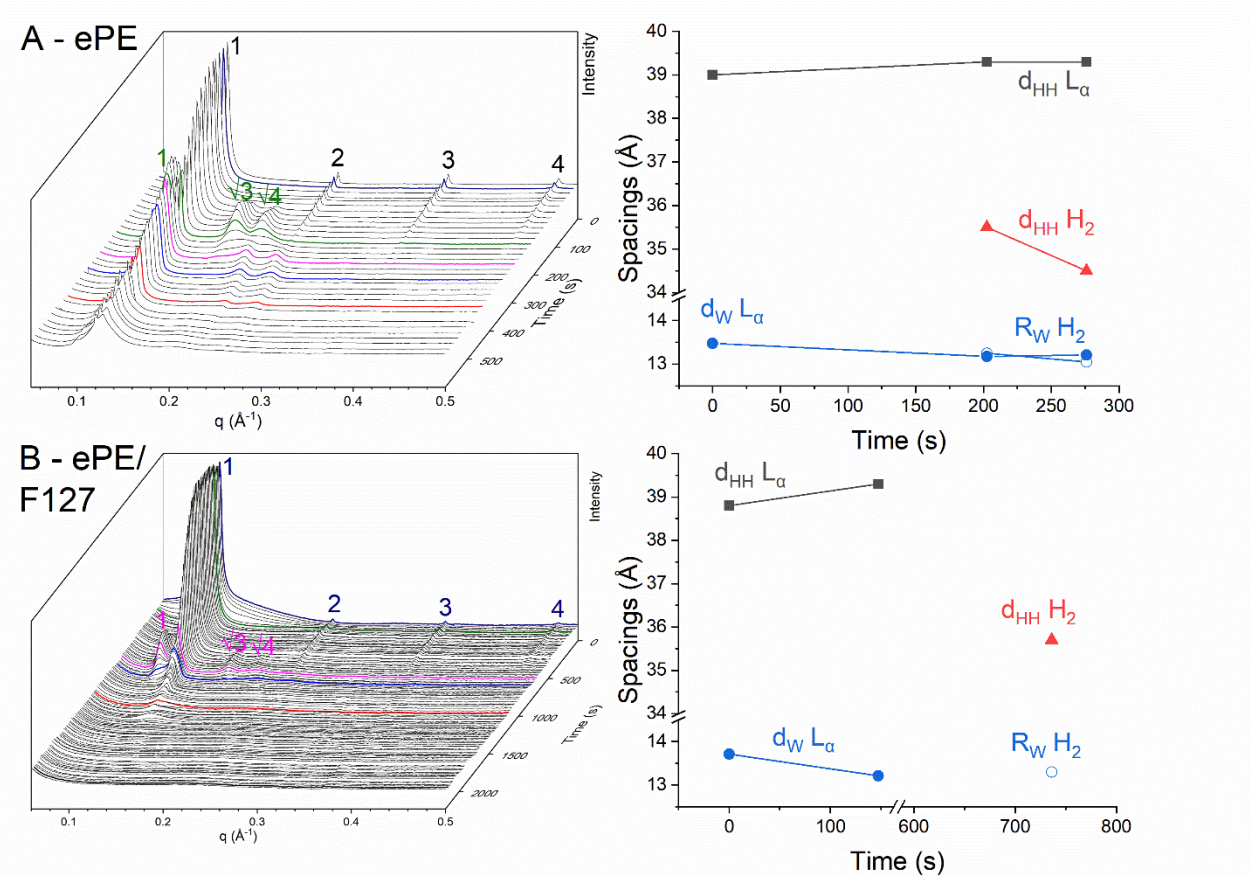

Fig. 2 – Left: time resolved SAXS intensity profiles showing the evolution of structure of egg phosphatidylethanolamine (ePE, top; panel A) and ePE dispersed in 0.5% Pluronic F127 (ePE/F127, bottom; panel B) during hydrolysis with PLC. Note: To avoid the obscuration of diffraction patterns with lower intensities, frames are plotted in inverse temporal order. Single SAXS intensity profiles highlighting key diffraction patterns during hydrolysis can be found in Fig. SI-4. Right: changes of structural parameters over time: the phospholipid headgroup-headgroup distance, d_{HH}, and water lamellae thickness, d_W, of the L_α phase, and the shortest headgroup-headgroup distance d_{HH} and radius of the water channel, R_W, of the H_{II} phase are given (for definitions see SI Materials and Methods and Fig. SI-2).

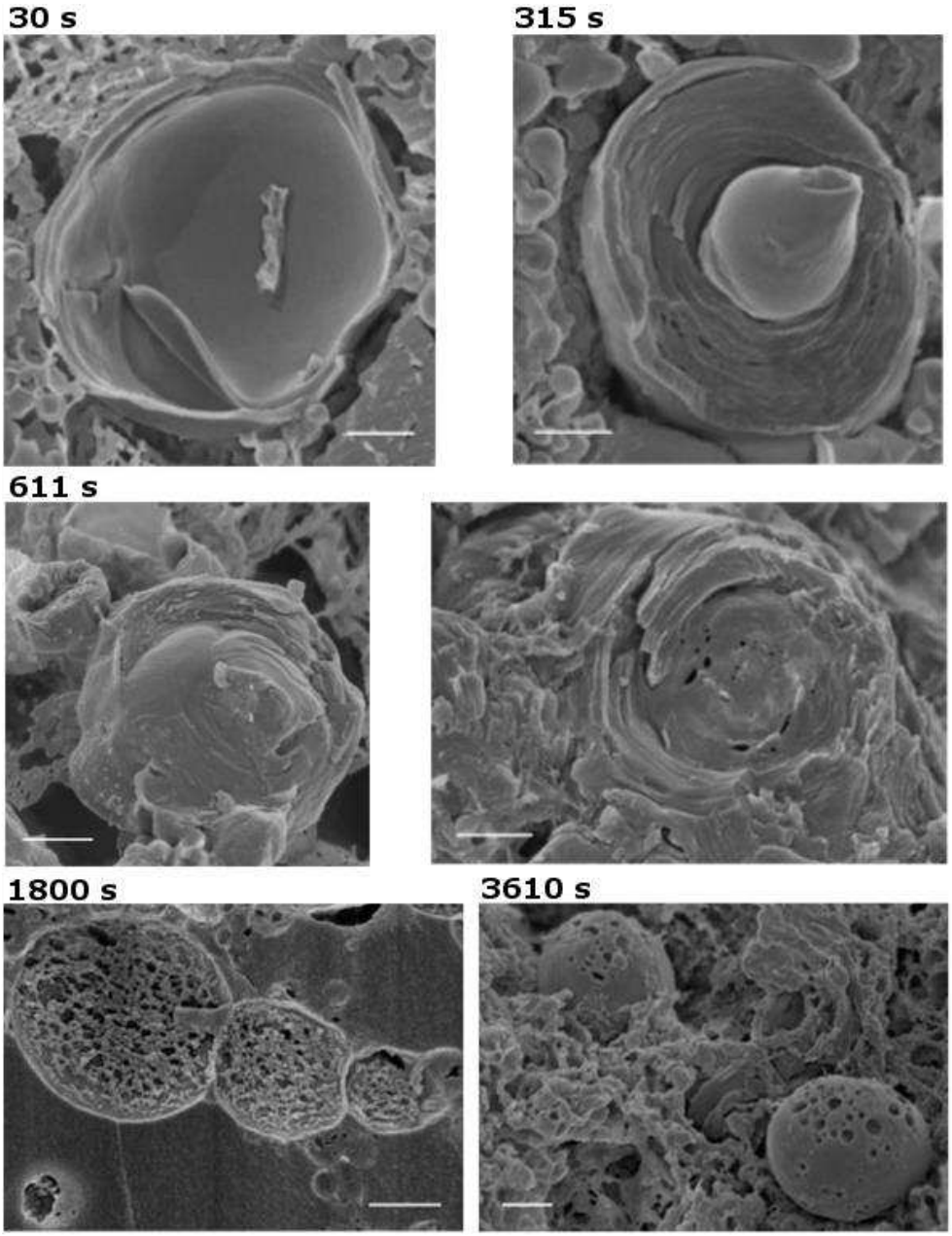

Fig. 3 – Representative cryoSEM images at selected time points showing the structure of structure of egg phosphatidylethanolamine dispersed in 0.5% F127 solution (ePE/F127) vesicles during PLC catalysed hydrolysis (scale bar = 500 nm). Additional representative SEM images can be found in the Fig. SI-5.

Structural changes resulting from PLC-catalysed hydrolysis of soy phosphatidylcholine (sPC)

PLC catalysed hydrolysis of sPC vesicles resulted in a decrease in intensity of the lamellar peaks without any significant change in lattice parameter of the lamellae over the course of hydrolysis, corresponding to a slight increase in d_{HH} coupled to a slight decrease in d_W (Fig. 4, top). This is in agreement with a previous study, however, a phase transition was not observed as was hypothesised by the authors.[27] We attribute the slight changes in the lamellar structure to the incorporation of a limited amount of DAG4 into the lipid bilayer. The separation of an oil phase was also observed, which was found to be reversible upon a large input of external energy; intense probe sonication was required for the insertion of DAG4 into the lipid bilayer and consequently the formation of the H_{II} phase (Fig. SI-6). The hydrolysis of sPC with phospholipases D (PLD) and phospholipases A2 (PLA2) also progressed without a change in nanostructure (Fig. SI-7); for brevity, this is further discussed in the SI.

The sPC/F127 dispersion was initially constituted of a mixture of vesicles and micelles. PLC catalysed hydrolysis resulted in a decrease in intensity of the lamellar peaks of the vesicles, accompanied by a massive growth in intensity at low q-values, an indication of the sequestration of the DAG4 into micellar structures that grow over time (Fig. 4, bottom). Interestingly, opposite trends in structural spacings were observed: a decrease in d_{HH} accompanied by an increase in d_W, which is attributed to the movement of the hydrophobic products of digestion into the growing micelles leading to an overall increase in membrane fluidity. The hydrolysis of sPC/F127 was also followed using cryoSEM (Fig. 5). At each time point, phase behaviour analogous to time-resolved SAXS was observed: (1) 10 s unilamellar vesicles; (2) 364 s small unilamellar vesicles and the phase separation and coalescence; (3) 680 s multilamellar vesicles, phase separation and coalescence; (4) 1935 s coalescence and the growth of oil droplets; and (5) 3630 s coalescence and the growth of oil droplets. Oil droplets were differentiated from vesicles by the lack the lamellar structure. The images at 680, 1935 and 3630 s were taken using both the in-lens and backscattered electron detectors to show the 3D aspects of the aggregating particles.

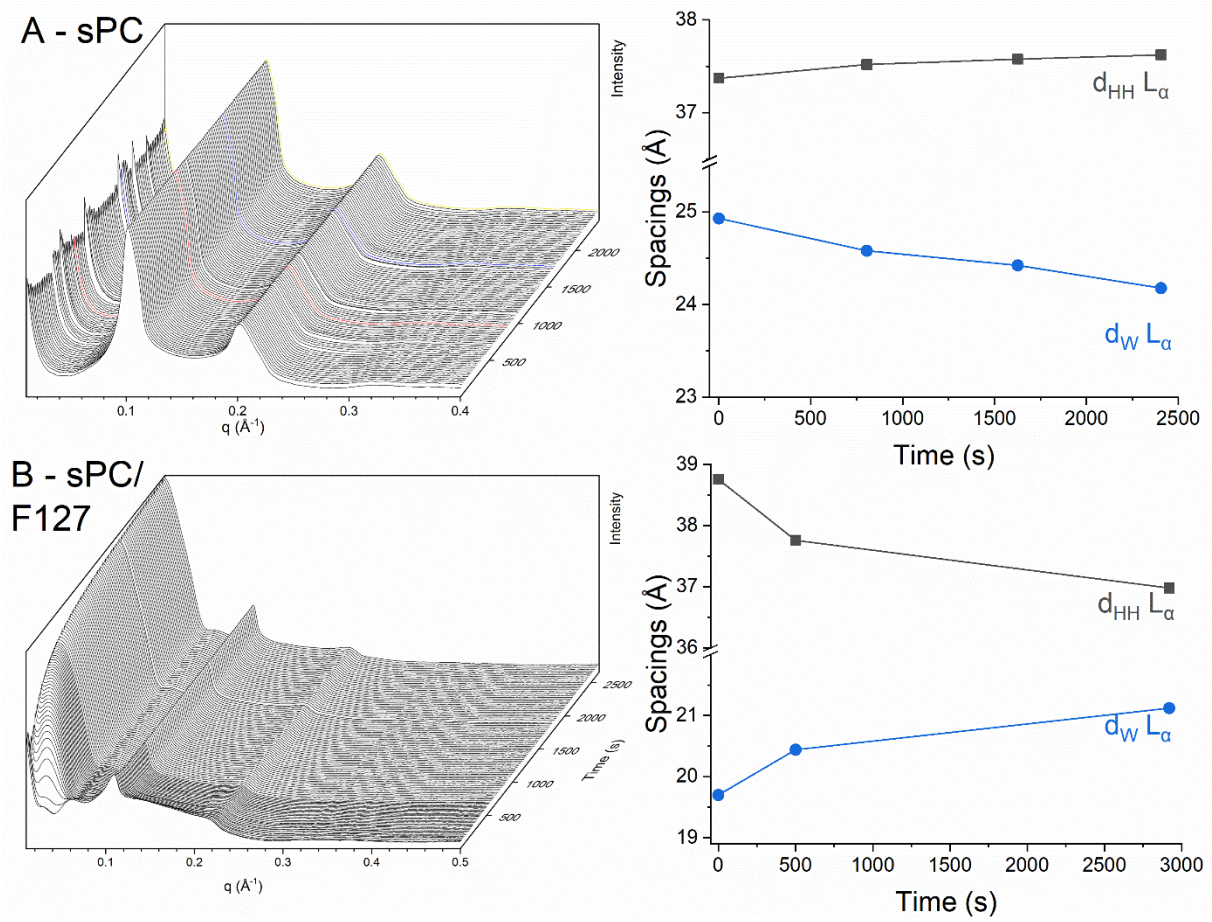

Fig. 4 –Left: time resolved SAXS intensity profiles showing the evolution of structure of soy phosphatidylcholine vesicles (sPC, top; panel A) and sPC dispersed in 0.5% F127 solution (sPC/F127, bottom; panel B) during hydrolysis with phospholipase. Right: membrane and water layer thicknesses over time. The phospholipid headgroup-headgroup distance, d_{HH}, and water lamellae thickness, d_W, of the L_α phases were determined in both cases by the '2-peak method' as described in the Methods section, SI pages 1-3 and references [22-23].

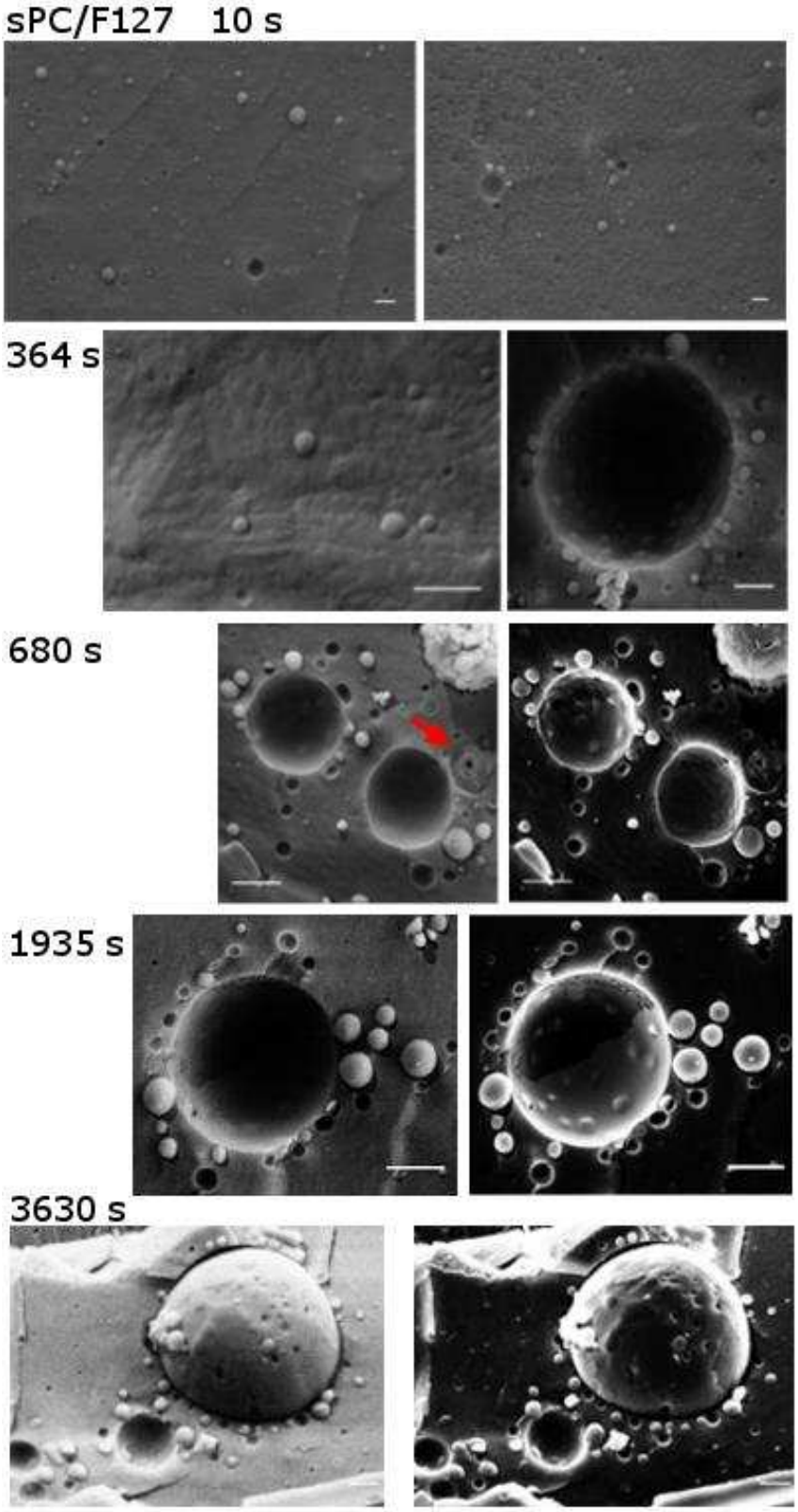

Fig. 5 – Representative cryoSEM images at selected time points showing the structure of soy phosphatidylcholine dispersed in 0.5% F127 solution (sPC/F127) vesicles during PLC catalysed hydrolysis (scale bar = 500 nm). At time points 680, 1935 and 3630 s, images of the same sample position are shown using both the in-lens and backscattered electron detectors in order to show the details of the surfaces in the depth of the image. A

multilamellar vesicle is indicated with a red arrow. Additional representative SEM images can be found in the Fig. SI-8.

Hydrolysis of ePE and sPC vesicles: quantification of hydrolysis products by NMR

Hydrolysis of the ePE vesicles occurs under two conditions and at two distinct rates (Fig. 6 and Table 2). The hydrolysis (H_1 = 49%) occurs at a faster rate of k_1 = 0.38 min^{-1} and with a proportion of the material (H_2 = 51%) hydrolysed at a rate about 50 times slower (k_2 = 0.0068 min^{-1}). Most of the hydrolysis occurred at a faster rate, with a smaller proportion of the material hydrolysed at a rate 50-fold slower. This second slower rate is attributed to the diffusion of lipids from within the vesicle to the lipid-water interface,[28-29] as this must occur before the lipids can be hydrolysed by PLC. A lag time that has previously been observed in PLC catalysed hydrolysis of lipids was not observed.[30]

The ePE particles in the absence of a stabiliser undergo hydrolysis at a slower rate and to a lower extent (56% of hydrolysis) by approximately 15%. The hydrolysis reaction occurs at a faster rate and greater extent (k_1 = 0.58 min^{-1} and H_1 = 74%; k_2 = 0.0017 min^{-1} and H_2 = 26%; 71% of hydrolysis), in the presence of the stabiliser. This reflects the stability of the ePE/F127 dispersions, which did not aggregate upon hydrolysis.

The increased rate of hydrolysis of the ePE/F127 formulation did not coincide with an increased rate of structural change when compared to the bare particles. Instead, nanostructural changes were observed to occur more slowly. The presence of the stabiliser prevented the aggregation of the nanostructured lipidic particles and could be participating in the lipid reorganisation thereby stabilising the system against a phase transition. The stabilised particles follow the same phase transitions as the bare particles, demonstrating that the steric hindrance provided by the surfactant does not alter the way the enzymes approach and hydrolyse the ePE at the interface.

Hydrolysis of sPC/F127 occurs in two environments and at two distinct rates (k_1 = 0.47 min^{-1} and H_1 = 35%; k_2 = 0.0027 min^{-1} and H_2 = 65%, Fig. 6 and Table 2), in the same fashion as the ePE formulations and with a hydrolysis yield of 38%. Note that the rate and extent of hydrolysis of the sPC formulation without stabiliser could not be determined due to phase separation and consequent inhomogeneity of the sample. The hydrolysis of sPC occurred mostly at the slower rate, which relates to the speed of translocation of the PC to the interface.[31-32] The hydrolysis also did not proceed to the same extent as in the ePE formulations, which is attributed to the system being saturated with product. In the ePE systems, the DAG1 product was 'removed' from the bulk by rearranging within the lipidic bilayer, whereas the DAG4 in the sPC/F127 system appeared to escape the lipid bilayer into large micellar structures.

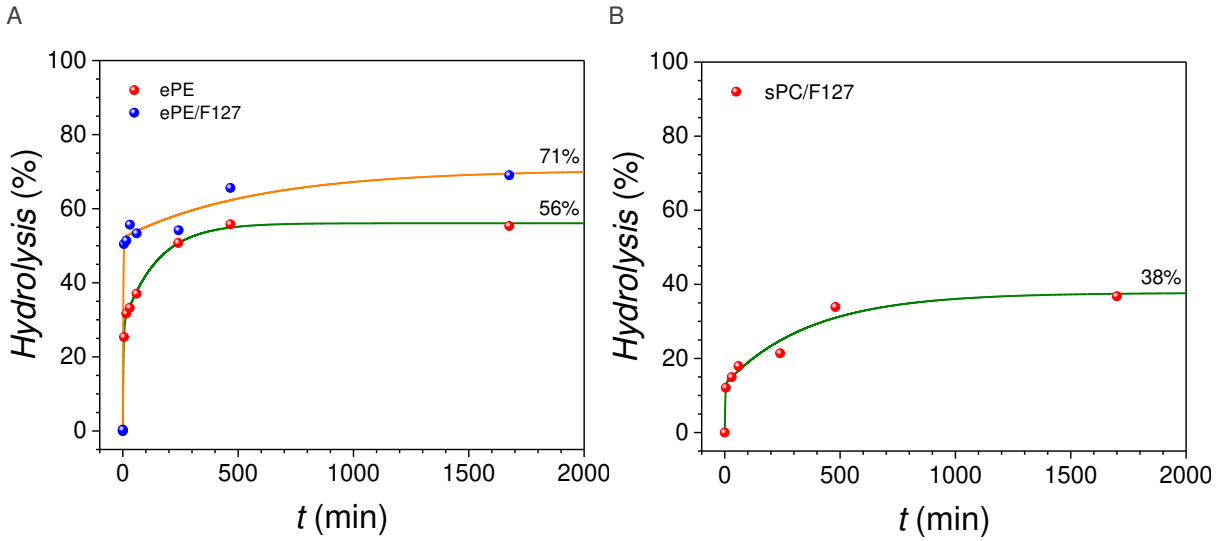

Fig. 6 – The extent of A. egg phosphatidylethanolamine hydrolysis with (ePE/F127) & without (ePE) stabiliser (Pluronic F127), and B. soy phosphatidylcholine with stabiliser (sPC/F127) by PLC as determined by ^{1}H NMR analysis. The solid line represents the fit of the data with equation (5) in the SI.

Table 2: The reaction rate (k) and extent (H) of hydrolysis of ePE and sPC formulations with PLC as determined by ^{1}H NMR, where H_1 and k_1 are attributed to hydrolysis occurring at the lipid-water interface, H_2 and k_2 to the diffusion of the phospholipid to the lipid-water interface, and H_{max} refers to the maximum amount of hydrolysis that occurs.

Formulation	H_1	k_1 (min^{-1})	H_2	k_2 (min^{-1})	H_{max}
ePE	49%	0.38	51%	0.0068	56%
ePE/F127	74%	0.58	26%	0.0017	71%
sPC/F127	35%	0.47	65%	0.0027	38%

Equilibrium phase behaviour of phospholipid dispersions

The equilibrium phase behaviour of ePE/F127 and sPC/F127 was studied to understand the potential of the systems to form non-equilibrium phases. At high temperatures, ePE/F127 intrinsically formed inverse phases – the inverse hexagonal phase, H_{II}, and the bicontinuous cubic phase with the space group Im3m (Fig. 7A and 7B) as previously observed.[33] On the other hand, sPC/F127 did not form inverse phases with an increase in temperature (Fig. 7C).

It has been previously shown that the incorporation of DAG into PC bilayers promotes the formation of inverse phases,[27, 34-35] which was not observed in the time-resolved SAXS studies. The deliberate incorporation of dilinolein, a model DAG which represents the majority product from the hydrolysis of sPC, into sPC vesicles resulted in the formation of inverse phases – the bicontinuous cubic phase with the space group Pn3m at 16 mol%, and then H_{II} phase at 29 mol% (Fig. 7D). The presence of DAG in the phospholipid bilayer favours negative bilayer curvature as their relatively small

headgroup allows them to position themselves deeper into the hydrophobic interior of the bilayer, where they modify the spacing between PC molecules that results in increased molecular ordering of the surrounding PC molecules and consequent reduction in the lateral diffusion of molecules.[36-37] Although the hydrolysis of the sPC progressed beyond 65 mol% in the dynamic studies, phase separation was observed, but not a phase transition, suggesting that it is more energetically favourable for DAG4 to phase separate than to reorganise within the sPC lipid bilayer.

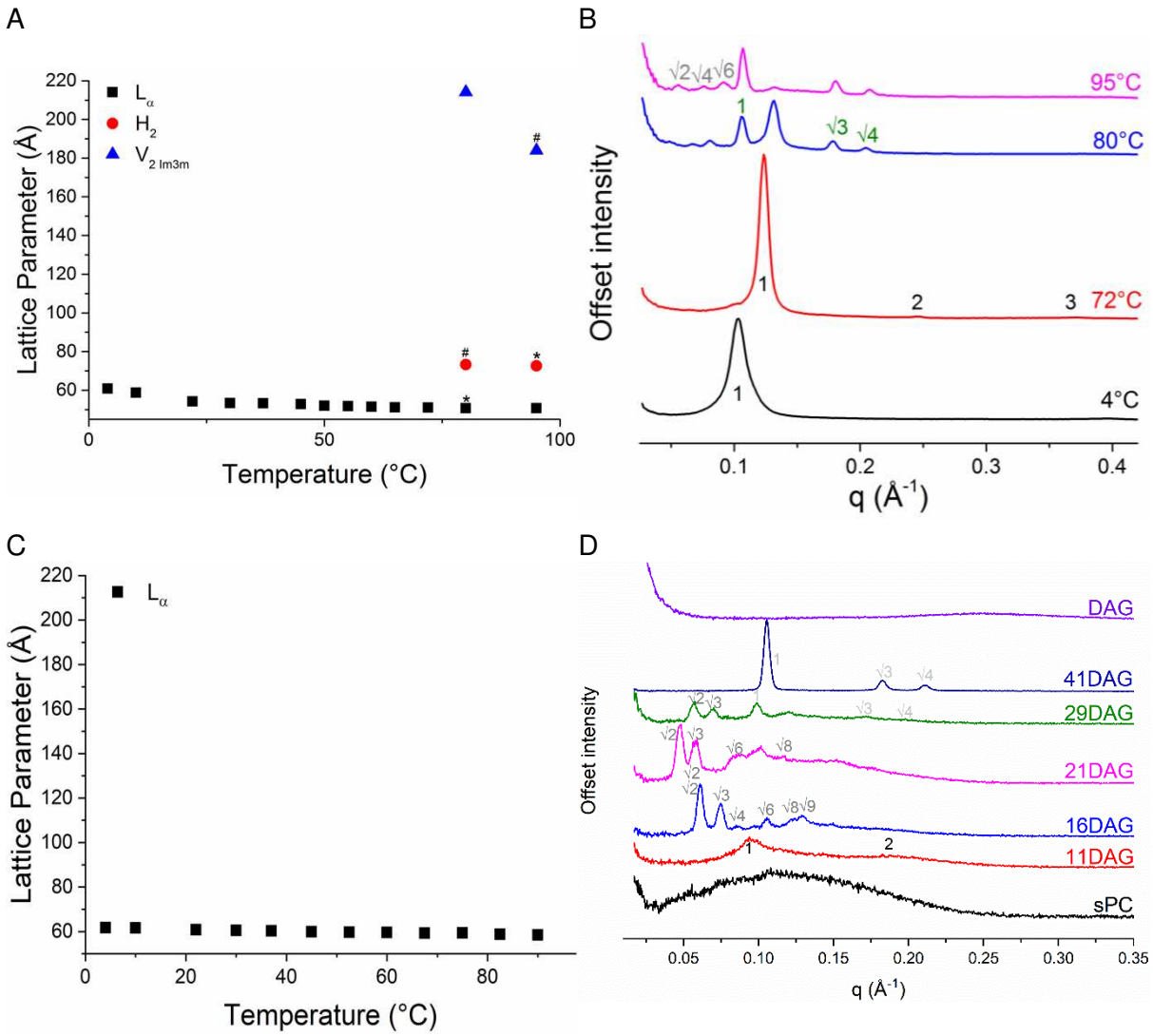

Fig. 7 – Equilibrium phase behaviour of dispersions of ePE/F127 and sPC/F127 without and with DAG. A. Temperature dependence of the phase behaviour of ePE/F127 without DAG. In coexistence regimes the asterisk (*) indicates most dominant mesophase and the second most intense phase is marked with a hash (#). B. Selected SAXS patterns that highlight the phase changes. C. Temperature dependence of the phase behaviour of sPC/F127 without DAG. D. Selected SAXS patterns of sPC/F127 containing increasing amounts of dilinolein. The reflections of the different liquid-crystalline phases are annotated in panel B and D for the L_α phase (black), for the bicontinuous cubic phases V_2 (grey) and for the H_{II} phase (green). The concentration of DAG (mol%) in sPC are indicated (right).

Discussion

In this study, the kinetics of PLC-catalysed lipid hydrolysis of ePE and sPC was observed, with a focus upon the dynamic nanostructures formed by the reorganisation of the hydrolysis products within the lipid bilayer. The presence of a non-ionic block copolymer surfactant, Pluronic F127, used to stabilise the lipid-water interface of the vesicle, mildly accelerated the rate and increased the extent of hydrolysis but did not prevent access of the enzyme to its substrate. The resulting phase behaviour differed greatly. ePE formed inverse phases, where the presence of the surfactant maintains the liquid-crystalline mesophases formed for a longer period. In comparison, sPC vesicles did not change in structure upon exposure to PLC, but the resulting DAG phase separates. Further, the presence of the stabiliser in the system results in the creation of micellar structures that grow over time due to the phase separation of the DAG and its subsequent incorporation into the micelles.

When both the ePE and sPC are hydrolysed, the removal of the phosphorylethanolamine or phosphorylcholine from the headgroup reduces the polarity of the amphiphile, thus removing the major barrier to trans-bilayer movement and allowing for the rapid equilibration of DAG within (and out of) the system.[38-40] What is demonstrated in this study is how bilayers comprising of the two different types of phospholipids respond to the stress induced by the production of DAG. Alone, DAG is a viscous liquid that is uncharged, extremely hydrophobic, and therefore immiscible with and highly buoyant in water. DAGs are normally minor lipid constituents in cells, but they play key roles in several biological processes, including as a second messenger in cellular signal transduction.[41] The interaction of DAGs with key phospholipids in lipid membranes potentially determines their biological fate, and will be discussed in terms of lipid incompatibility and its effect on the membrane curvature.

It was observed that DAG deliberately incorporated into sPC lipidic bilayers in the equilibrium studies behave differently to dynamically produced DAG4 via PLC hydrolysis. The phase separation of the DAG4 is a consequence of increased hydrophobicity upon removal of the headgroup, particularly given that the acyl chains are >10 carbons in length (Table 1).[42] It was initially thought that the distribution of DAG during the digestion process could be anticipated by using this equilibrium phase behaviour as a calibration as previously demonstrated with light sensitive inverse phases.[43] However, this was not the case due to the nature of the phase transition at play in this system: from lamellar vesicles to the H_{II} phase. This is a phase transition that phospholipid bilayers generally try to avoid as energetically unfavourable changes must occur for the transformation to proceed, namely, changes in curvature, the formation of voids in the hydrophobic core and the exposition of lipid chains to interbilayer water.[25, 44] The avoidance of the formation of H_{II} phase has also been observed in bicontinuous cubic nanostructures.[45-46] By preforming the lipid particles at equilibrium, these phenomena are avoided. Moreover, the complexity of this biological system – the interfacial nature of the enzyme and the effect

of the other product of enzyme action, phosphorylcholine and phosphorylethanolamine, upon the colloidal stability of the particle cannot be reproduced at equilibrium.

The evolution and phase separation of DAG in sPC bilayers did not result in a phase transition to inverse phases as demonstrated in equilibrium studies. Instead, DAG escapes from the lipid bilayer, which is attributed to a mismatch in molecular shape and hydrophobicity, and a limited capability to form hydrogen bonds. It is not possible for the $^{-}$OH group of the DAG4 molecule to form hydrogen bonds with the $RN(CH_3)_3^+$ moiety of the sPC headgroup as trimethyl ammonium moieties cannot act as a hydrogen bond donor group. This absence of hydrogen bonding interaction was confirmed by molecular simulations (Fig. SI-9). This molecular behaviour allows for DAG to act as a mobile messenger. Moreover, this effect may be exaggerated by the fluidity of the linoleic acid chains of the sPC,[47-48] as compared to the palmitoyl/oleoyl chains of the ePE. The speed of lipid movement may also play a role in the reorganisation of the lipidic bilayer. The spontaneous translocation of phospholipids across the bilayer has been estimated to be extremely slow (10^{-15} s^{-1}),[31] a process that is influenced by membrane fluidity as well as size of the lipid that is moving.[32] The translocation of the smaller, hydrophobic DAG molecules occurs much faster (63 s^{-1}),[49] where this mismatch in speed may add to the propensity for phase separation. Thus, in the case of sPC, it is more favourable for the DAG to escape from the bilayer as a DAG-rich second phase than to reorganise within the vesicle lipid bilayers.

In contrast, ePE bilayers incorporated the DAG produced by PLC hydrolysis into the lipid bilayer, resulting in the formation of negative curvature. This follows their intrinsic ability to form inverse phases. The production of DAG forces the partial dehydration of the headgroups and an increase in the hydrophobic volume.[47] The DAG1 is able to stay within the ePE bilayer, as the $^{-}$OH group of the DAG1 is able to establish hydrogen bonds with the donor RNH_3^+group on the PE headgroup, as confirmed by molecular simulations (Fig. SI-10). The resulting phase transition from L_α to H_{II} results from the dynamic equalisation between the free energy of hydrocarbon chain packing and the curvature energy, a function of electrostatic interactions and hydration.[50-51] In the absence of the surfactant, the vesicles are able to fuse as there is no barrier to the formation of a highly curved bridge between the multilamellar vesicles.[52]

The most significant differences between the behaviour of PCs and PEs relate to the behaviour of their headgroups at the interface. Reported and experimental differences between the headgroups of PE and PC are shown in Table 2 and reported in Figs 2 and 4. PC bilayers have a larger bilayer thickness (d_{HH}) as well as separation (d_W) than PE bilayers. Interestingly, the presence of the stabiliser in the sPC bilayer seems to increase d_{HH} and reduce the d_W. This is attributed to a slight reduction of membrane fluidity in the presence of a stabiliser, and hence leading to reduction in undulation-caused repulsion forces going hand in hand with a reduction in the interlamellar distance, d_W. The large headgroup area of PCs prevents the formation of inverse phases, whereas the reduced headgroup area of the PE results

in smaller d_W and decreased mean square membrane fluctuations by factor of 2-4 (referring to the Caillé parameter).[53-55]

Table 2 – Molecular dimensions from literature comparing features of the PC and PE headgroups.[56-57]

	PC	PE
Headgroup diameter (Å)	10	8
Headgroup size (Å^3)	344	246
Bulk water/lipid molecule	23	12

In the formulation of new drug delivery systems, it is important to keep in mind that static models cannot be solely relied upon to predict their fate in vivo. The human body is a complex machine in which most biochemical reactions are constantly changing, including the ones involving the digestions of drugs and their delivery systems. Consequently, their kinetic states and are not in thermodynamic equilibrium.

Conclusions

This study gives insights into the manipulation of lipidic membranes in response to exposure to phospholipase C. The roles of phosphatidylcholines and phosphatidylethanolamines within a lipid bilayer differ greatly. Bilayers formed by the two phospholipids respond to the stress of hydrolysis in two different ways. The mismatch of the DAG molecules and sPC causes the escape of the produced DAG4 due to poor interaction with the remaining sPC molecules in the lipid bilayer; whereas the produced DAG1 molecules contributes to the creation of negative curvature in the ePE bilayer as they remained in the bilayer due to hydrogen bonding. This contrasts with what was observed at equilibrium and has been observed in the literature, highlighting that dynamic self-assembly of lipids cannot be predicted by equilibrium models. As can be seen, the chemistry of the phospholipid head group plays an important role in the fate of the DAG. From a biophysics point of view, this study supports the consensus that the formation of lipid domains play essential roles in cellular response to stress. The DAG produced from a PC rich domain is more likely to escape the lipid bilayer, whereas the DAG produced in a PE rich domain is likely to be retained within the lipid bilayer and so influence lipid packing through dehydration and expansion of the lipidic volume. This study links the biochemical changes in PE and PC membranes that are required to effect cellular fusion and intracellular signalling; phenomena that can be tuned to deliberately trigger phase transitions in lyotropic liquid-crystalline materials that mimic physiological responses to disease states.

Acknowledgements

WKF was the recipient of a Victorian Postdoctoral Research Fellowship. This work benefitted from support from the Swiss National Science Foundation through the National Center of Competence

in Research Bio-Inspired Materials. Part of this research was undertaken on the SAXS/WAXS beamline at the Australian Synchrotron. The authors acknowledge support of the Scientific Center for Optical and Electron Microscopy ScopeM of the Swiss Federal Institute of Technology ETHZ.

Current address

[1]WKF: Chemistry, School of Environmental & Life Sciences, The University of Newcastle, Callaghan, NSW, 2308 Australia.

References

1. Kossena, G. A.; Charman, W. N.; Boyd, B. J.; Dunstan, D. E.; Porter, C. J., Probing drug solubilization patterns in the gastrointestinal tract after administration of lipid-based delivery systems: a phase diagram approach. *J Pharmaceut Sci* **2004,** *93* (2), 332-48.
2. Kossena, G. A.; Charman, W. N.; Boyd, B. J.; Porter, C. I. H., Influence of the intermediate digestion phases of common formulation lipids on the absorption of a poorly water-soluble drug. *J Pharm Sci-Us* **2005,** *94* (3), 481-492.
3. Thomas, N.; Holm, R.; Rades, T.; Mullertz, A., Characterising Lipid Lipolysis and Its Implication in Lipid-Based Formulation Development. *Aaps J* **2012,** *14* (4), 860-871.
4. Fong, W. K.; Hanley, T.; Boyd, B. J., Stimuli responsive liquid crystals provide 'on-demand' drug delivery in vitro and in vivo. *J Control Release* **2009,** *135* (3), 218-226.
5. Zabara, A.; Mezzenga, R., Controlling molecular transport and sustained drug release in lipid-based liquid crystalline mesophases. *J Control Release* **2014,** *188*, 31-43.
6. Fong, W.-K.; Negrini, R.; Vallooran, J. J.; Mezzenga, R.; Boyd, B. J., Responsive self-assembled nanostructured lipid systems for drug delivery and diagnostics. *Journal of Colloid and Interface Science* **2016,** *484*, 320-339.
7. Negrini, R.; Mezzenga, R., pH-Responsive Lyotropic Liquid Crystals for Controlled Drug Delivery. *Langmuir* **2011,** *27* (9), 5296-5303.
8. Phan, S.; Salentinig, S.; Hawley, A.; Boyd, B. J., How relevant are assembled equilibrium samples in understanding structure formation during lipid digestion? *Eur J Pharm Biopharm* **2015,** *96*, 117-124.
9. Phan, S.; Hawley, A.; Mulet, X.; Waddington, L.; Prestidge, C. A.; Boyd, B. J., Structural Aspects of Digestion of Medium Chain Triglycerides Studied in Real Time Using sSAXS and Cryo-TEM. *Pharm Res-Dordr* **2013,** *30* (12), 3088-3100.
10. Borne, J.; Nylander, T.; Khan, A., Effect of lipase on monoolein-based cubic phase dispersion (cubosomes) and vesicles. *J Phys Chem B* **2002,** *106* (40), 10492-10500.
11. Salentinig, S.; Phan, S.; Khan, J.; Hawley, A.; Boyd, B. J., Formation of Highly Organized Nanostructures during the Digestion of Milk. *Acs Nano* **2013,** *7* (12), 10904-10911.
12. Fong, W. K.; Salentinig, S.; Prestidge, C. A.; Mezzenga, R.; Hawley, A.; Boyd, B. J., Generation of geometrically ordered lipid-based liquid-crystalline nanoparticles using biologically relevant enzymatic processing. *Langmuir* **2014,** *30* (19), 5373-7.
13. Fong, W.-K.; Sanchez-Ferrer, A.; Ortelli, F. G.; Sun, W.; Boyd, B. J.; Mezzenga, R., Dynamic formation of nanostructured particles from vesicles via invertase hydrolysis for on-demand delivery. *RSC Advances* **2017,** *7* (8), 4368-4377.
14. Hong, L. D.; Salentinig, S.; Hawley, A.; Boyd, B. J., Understanding the Mechanism of Enzyme-Induced Formation of Lyotropic Liquid Crystalline Nanoparticles. *Langmuir* **2015,** *31* (24), 6933-6941.
15. Cocco, L.; Follo, M. Y.; Manzoli, L.; Suh, P.-G., Phosphoinositide-specific phospholipase C in health and disease. *Journal of Lipid Research* **2015,** *56* (10), 1853-1860.
16. Kadamur, G.; Ross, E. M., Mammalian Phospholipase C. *Annual Review of Physiology* **2013,** *75* (1), 127-154.
17. Yang, Y. R.; Kang, D.-S.; Lee, C.; Seok, H.; Follo, M. Y.; Cocco, L.; Suh, P.-G., Primary phospholipase C and brain disorders. *Advances in Biological Regulation* **2016,** *61*, 80-85.
18. Koss, H.; Bunney, T. D.; Behjati, S.; Katan, M., Dysfunction of phospholipase Cγ in immune disorders and cancer. *Trends in Biochemical Sciences* **2014,** *39* (12), 603-611.

19. Warren, D. B.; Anby, M. U.; Hawley, A.; Boyd, B. J., Real Time Evolution of Liquid Crystalline Nanostructure during the Digestion of Formulation Lipids Using Synchrotron Small-Angle X-ray Scattering. *Langmuir* **2011,** *27* (15), 9528-9534.
20. Kirby, N. M.; Mudie, S. T.; Hawley, A. M.; Cookson, D. J.; Mertens, H. D. T.; Cowieson, N.; Samardzic-Boban, V., A low-background-intensity focusing small-angle X-ray scattering undulator beamline. *J Appl Crystallogr* **2013,** *46*, 1670-1680.
21. Hyde, S. T., Identification of lyotropic liquid crystalline mesophases. In *Handbook of Applied Surface and Colloid Chemistry*, Holmberg, K., Ed. John Wiley & Sons: 2002.
22. Li, N. Y. D.; Perutkova, S.; Iglic, A.; Rappolt, M., My first electron density map: A beginner's guide to small angle X-ray diffraction. *Elektroteh Vestn* **2017,** *84* (3), 69-75.
23. Rappolt, M., Bilayer thickness estimations with "poor" diffraction data. *J Appl Phys* **2010,** *107* (8).
24. Luzzati, V.; Husson, F., The structure of the liquid-crystalline phases of lipid-water systems. *The Journal of Cell Biology* **1962,** *12* (2), 207-219.
25. Rappolt, M.; Hickel, A.; Bringezu, F.; Lohner, K., Mechanism of the lamellar/inverse hexagonal phase transition examined by high resolution x-ray diffraction. *Biophysical journal* **2003,** *84* (5), 3111-3122.
26. Goñi, F. M.; Alonso, A., Structure and functional properties of diacylglycerols in membranes. *Progress in Lipid Research* **1999,** *38* (1), 1-48.
27. Holme, M. N.; Rashid, M. H.; Thomas, M. R.; Barriga, H. M. G.; Herpoldt, K. L.; Heenan, R. K.; Dreiss, C. A.; Bañuelos, J. L.; Xie, H.-n.; Yarovsky, I.; Stevens, M. M., Fate of Liposomes in the Presence of Phospholipase C and D: From Atomic to Supramolecular Lipid Arrangement. *ACS Central Science* **2018,** *4* (8), 1023-1030.
28. Allan, D.; Thomas, P.; Michell, R. H., Rapid transbilayer diffusion of 1,2-diacylglycerol and its relevance to control of membrane curvature. *Nature* **1978,** *276*, 289.
29. Fong, W. K.; Hanley, T. L.; Thierry, B.; Hawley, A.; Boyd, B. J.; Landersdorfer, C. B., External manipulation of nanostructure in photoresponsive lipid depot matrix to control and predict drug release in vivo. *J Control Release* **2016,** *228*, 67-73.
30. Goñi, F. M.; Montes, L. R.; Alonso, A., Phospholipases C and sphingomyelinases: Lipids as substrates and modulators of enzyme activity. *Progress in Lipid Research* **2012,** *51* (3), 238-266.
31. Nakano, M.; Fukuda, M.; Kudo, T.; Endo, H.; Handa, T., Determination of Interbilayer and Transbilayer Lipid Transfers by Time-Resolved Small-Angle Neutron Scattering. *Physical Review Letters* **2007,** *98* (23), 238101.
32. Nakano, M.; Fukuda, M.; Kudo, T.; Matsuzaki, N.; Azuma, T.; Sekine, K.; Endo, H.; Handa, T., Flip-Flop of Phospholipids in Vesicles: Kinetic Analysis with Time-Resolved Small-Angle Neutron Scattering. *The Journal of Physical Chemistry B* **2009,** *113* (19), 6745-6748.
33. Cullis, P. R.; de Kruijff, B., The polymorphic phase behaviour of phosphatidylethanolamines of natural and synthetic origin. A 31P NMR study. *Biochimica et biophysica acta* **1978,** *513* (1), 31-42.
34. Basáñez, G.; Ruiz-Argüello, M. B.; Alonso, A.; Goñi, F. M.; Karlsson, G.; Edwards, K., Morphological changes induced by phospholipase C and by sphingomyelinase on large unilamellar vesicles: a cryo-transmission electron microscopy study of liposome fusion. *Biophysical Journal* **1997,** *72* (6), 2630-2637.
35. Nieva, J. L.; Alonso, A.; Basáñez, G.; Goñi, F. M.; Gulik, A.; Vargas, R.; Luzzati, V., Topological properties of two cubic phases of a phospholipid : cholesterol: diacylglycerol aqueous system and their possible implications in the phospholipase C-induced liposome fusion. *FEBS Letters* **1995,** *368* (1), 143-147.
36. Schorn, K.; Marsh, D., Lipid chain dynamics in diacylglycerol-phosphatidylcholine mixtures studied by slow-motional simulations of spin label ESR spectra. *Chemistry and Physics of Lipids* **1996,** *82* (1), 7-14.
37. Alwarawrah, M.; Dai, J.; Huang, J., Modification of Lipid Bilayer Structure by Diacylglycerol: A Comparative Study of Diacylglycerol and Cholesterol. *Journal of Chemical Theory and Computation* **2012,** *8* (2), 749-758.
38. Ganong, B. R.; Bell, R. M., Transmembrane movement of phosphatidylglycerol and diacylglycerol sulfhydryl analogues. *Biochemistry* **1984,** *23* (21), 4977-83.
39. Nieva, J. L.; Goni, F. M.; Alonso, A., Liposome fusion catalytically induced by phospholipase C. *Biochemistry* **1989,** *28* (18), 7364-7.
40. Ibarguren, M.; Bomans, P. H. H.; Frederik, P. M.; Stonehouse, M.; Vasil, A. I.; Vasil, M. L.; Alonso, A.; Goñi, F. M., End-products diacylglycerol and ceramide modulate membrane fusion induced by a phospholipase C/sphingomyelinase from Pseudomonas aeruginosa. *Biochimica et Biophysica Acta (BBA) - Biomembranes* **2010,** *1798* (1), 59-64.
41. Nishizuka, Y., The role of protein kinase C in cell surface signal transduction and tumour promotion. *Nature* **1984,** *308*, 693.
42. De Boeck, H.; Zidovetzki, R., Interactions of saturated diacylglycerols with phosphatidylcholine bilayers: a deuterium NMR study. *Biochemistry* **1992,** *31* (2), 623-630.

43. Fong, W.-K.; Hanley, T. L.; Thierry, B.; Kirby, N.; Boyd, B. J., Plasmonic Nanorods Provide Reversible Control over Nanostructure of Self-Assembled Drug Delivery Materials. *Langmuir* **2010,** *26* (9), 6136-6139.
44. Kozlov, M. M.; Leikin, S.; Rand, R. P., Bending, hydration and interstitial energies quantitatively account for the hexagonal-lamellar-hexagonal reentrant phase transition in dioleoylphosphatidylethanolamine. *Biophysical journal* **1994,** *67* (4), 1603-1611.
45. Tilley, A.; Dong, Y.-D.; Amenitsch, H.; Rappolt, M.; Boyd, B. J., Transfer of lipid and phase reorganisation in self-assembled liquid crystal nanostructured particles based on phytantriol. *Physical Chemistry Chemical Physics* **2011,** *13* (8), 3026-3032.
46. Moitzi, C.; Guillot, S.; Fritz, G.; Salentinig, S.; Glatter, O., Phase Reorganization in Self-Assembled Systems Through Interparticle Material Transfer. *Advanced Materials* **2007,** *19* (10), 1352-1358.
47. Alwarawrah, M.; Hussain, F.; Huang, J., Alteration of lipid membrane structure and dynamics by diacylglycerols with unsaturated chains. *Biochimica et Biophysica Acta (BBA) - Biomembranes* **2016,** *1858* (2), 253-263.
48. Szule, J. A.; Fuller, N. L.; Rand, R. P., The effects of acyl chain length and saturation of diacylglycerols and phosphatidylcholines on membrane monolayer curvature. *Biophys J* **2002,** *83* (2), 977-84.
49. Hamilton, J. A.; Bhamidipati, S. P.; Kodali, D. R.; Small, D. M., The interfacial conformation and transbilayer movement of diacylglycerols in phospholipid bilayers. *Journal of Biological Chemistry* **1991,** *266* (2), 1177-1186.
50. Gruner, S. M., Stability of lyotropic phases with curved interfaces. *The Journal of Physical Chemistry* **1989,** *93* (22), 7562-7570.
51. Kirk, G. L.; Gruner, S. M., Lyotropic Effects of Alkanes and Headgroup Composition on the L-Alpha-Hii Lipid Liquid-Crystal Phase-Transition - Hydrocarbon Packing Versus Intrinsic Curvature. *J Phys-Paris* **1985,** *46* (5), 761-769.
52. Markin, V. S.; Kozlov, M. M.; Borovjagin, V. L., On the theory of membrane fusion. The stalk mechanism. *Gen Physiol Biophys* **1984,** *3* (5), 361-77.
53. Rappolt, M.; Laggner, P.; Pabst, G., Structure and elasticity of phospholipid bilayers in the Lα phase: A comparison of phosphatidylcholine and phosphatidylethanolamine membranes. In *Recent Res. Devel. Biophys.*, Transworld Research Network: 2004; Vol. 3.
54. Kucerka, N.; van Oosten, B.; Pan, J. J.; Heberle, F. A.; Harroun, T. A.; Katsaras, J., Molecular Structures of Fluid Phosphatidylethanolamine Bilayers Obtained from Simulation-to-Experiment Comparisons and Experimental Scattering Density Profiles. *J Phys Chem B* **2015,** *119* (5), 1947-1956.
55. Pink, D. A.; McNeil, S.; Quinn, B.; Zuckermann, M. J., A model of hydrogen bond formation in phosphatidylethanolamine bilayers. *Biochimica et Biophysica Acta (BBA) - Biomembranes* **1998,** *1368* (2), 289-305.
56. Wilkinson, D. A.; Nagle, J. F., Dilatometry and calorimetry of saturated phosphatidylethanolamine dispersions. *Biochemistry* **1981,** *20* (1), 187-192.
57. McIntosh, T. J., Hydration properties of lamellar and non-lamellar phases of phosphatidylcholine and phosphatidylethanolamine. *Chemistry and Physics of Lipids* **1996,** *81* (2), 117-131.

Table of contents graphic

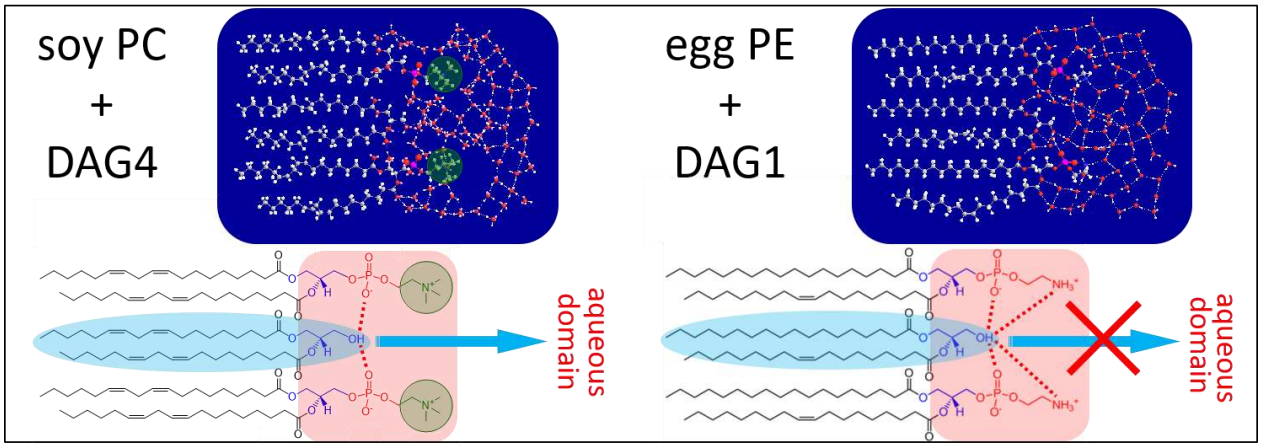

Towards understanding the in vivo fate of lipid-based drug delivery systems, this study looks at the structural consequences of PLC catalysed hydrolysis of phospholipid bilayers. Structural transformations of vesicles are determined by the movement of hydrophobic products which, in turn, are dependent on the ability of the headgroup to form hydrogen bonds.